Article

An Exchange-Free Measure of ^{15}N Transverse Relaxation: An NMR Spectroscopy Application to the Study of a Folding Intermediate with Pervasive Chemical Exchange

D. Flemming Hansen, Daiwen Yang, Haniqiao Feng, Zheng Zhou, Silke Wiesner, Yawen Bai, and Lewis E. Kay

J. Am. Chem. Soc., **2007**, 129 (37), 11468-11479• DOI: 10.1021/ja072717t • Publication Date (Web): 28 August 2007

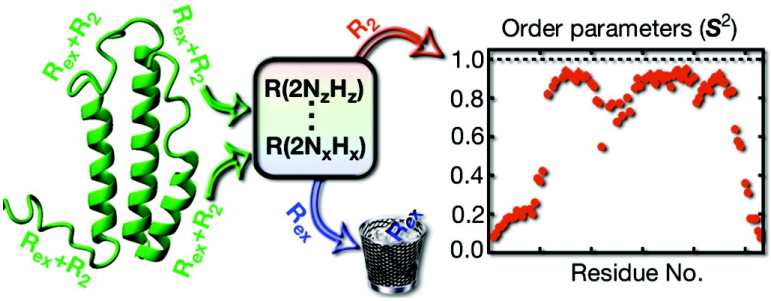

More About This Article

Additional resources and features associated with this article are available within the HTML version:

- Supporting Information
- Links to the 3 articles that cite this article, as of the time of this article download
- Access to high resolution figures
- Links to articles and content related to this article
- Copyright permission to reproduce figures and/or text from this article

View the Full Text HTML

J|A|C|S
ARTICLES
Published on Web 08/28/2007

An Exchange-Free Measure of ^{15}N Transverse Relaxation: An NMR Spectroscopy Application to the Study of a Folding Intermediate with Pervasive Chemical Exchange

D. Flemming Hansen,[†] Daiwen Yang,[‡] Haniqiao Feng,[§] Zheng Zhou,[§] Silke Wiesner,[||] Yawen Bai,[§] and Lewis E. Kay*[,†]

Contribution from the Departments of Medical Genetics, Biochemisty and Chemistry, The University of Toronto, Toronto, Ontario, Canada, M5S 1A8, Department of Biological Sciences, National University of Singapore, Singapore 117543, Laboratory of Biochemistry and Molecular Biology, Center for Cancer Research, NCI, NIH, Bethesda, Maryland 20892, and Structural Biology and Biochemistry, The Hospital for Sick Children, 555 University Avenue, Toronto, Ontario, Canada, M5G 1X8

Received April 18, 2007; E-mail: kay@pound.med.utoronto.ca

Abstract: A series of experiments are presented that provide an exchange-free measure of dipole−dipole ^{15}N transverse relaxation, R_{dd}, that can then be substituted for ^{15}N $R_{1\rho}$ or R_2 rates in the study of internal protein dynamics. The method is predicated on the measurement of a series of relaxation rates involving ^{1}H−^{15}N longitudinal order, anti-phase ^{1}H and ^{15}N single-quantum coherences, and ^{1}H−^{15}N multiple quantum coherences; the relaxation rates of all coherences are measured under conditions of spin-locking. Results from detailed simulations and experiments on a number of protein systems establish that R_{dd} values are independent of exchange and systematic errors from dipolar interactions with proximal protons are calculated to be less than 1−2%, on average, for applications to perdeuterated proteins. Simulations further indicate that the methodology is rather insensitive to the exact level of deuteration so long as proteins are reasonably highly deuterated (>50%). The utility of the methodology is demonstrated with applications involving protein L, ubiquitin, and a stabilized folding intermediate of apocytochrome b_{562} that shows large contributions to ^{15}N $R_{1\rho}$ relaxation from chemical exchange.

Introduction

Protein molecules are dynamic over a wide range of time scales, and it is becoming increasingly clear that there is often a strong relationship between these dynamics and biological function.[1] This has led to the development of a variety of different methodologies that probe motion in biomolecules, including both ensemble averaged[2−5] and single molecule experimental approaches[6] as well as computational techniques.[7] Heteronuclear NMR spin relaxation methods are among the most powerful since site-specific dynamics information is available over a large range of time scales extending from picoseconds to seconds.[8−11] A significant body of such experiments have emerged over the past decade, measuring many different auto- and cross-correlated spin relaxation rates in proteins involving a variety of different spin pairs.[12−18]

Nevertheless, the experiments that remain the most popular are among the earliest developed, namely those that extract backbone dynamics information from heteronuclear ^{1}H−^{15}N relaxation measurements.[8] These experiments typically involve quantifying heteronuclear longitudinal, R_1, and transverse, R_2, relaxation rates as well as the steady-state ^{1}H−^{15}N heteronuclear NOE that is obtained by comparing ^{15}N signal intensities in the presence and absence of ^{1}H saturation. The data are most frequently interpreted in terms of order parameters squared (S^2) and effective correlation times (τ_e) that describe the amplitudes and time constants of the motion, respectively.[19,20] Order

[†] The University of Toronto.
[‡] National University of Singapore.
[§] NCI, NIH.
[||] The Hospital for Sick Children.

(1) Karplus, M.; Kuriyan, J. *Proc. Natl. Acad. Sci. U.S.A.* **2005**, *102*, 6679−6685.
(2) Ishima, R.; Torchia, D. A. *Nat. Struct. Biol.* **2000**, *7*, 740−743.
(3) Hubbell, W. L.; Cafiso, D. S.; Altenbach, C. *Nat. Struct. Biol.* **2000**, *7*, 735−739.
(4) Selvin, P. R. *Nat. Struct. Biol.* **2000**, *7*, 730−734.
(5) Saibil, H. R. *Nat. Struct. Biol.* **2000**, *7*, 711−714.
(6) Yeung, E. S. *Annu. Rev. Phys. Chem.* **2004**, *55*, 97−126.
(7) Rapaport, D. C. *The Art of Molecular Dynamics Simulation*, 2nd ed.; Cambridge University Press: 2004.
(8) Kay, L. E.; Torchia, D. A.; Bax, A. *Biochemistry* **1989**, *28*, 8972−8979.
(9) Palmer, A. G.; Williams, J.; McDermott, A. *J. Phys. Chem.* **1996**, *100*, 13293−13310.
(10) Dayie, K. T.; Wagner, G.; Lefevre, J. F. *Annu. Rev. Phys. Chem.* **1996**, *47*, 243−282.
(11) Kay, L. E. *Nat. Struct. Biol.* **1998**, *5*, 513−517.
(12) Pang, Y. X.; Zuiderweg, E. R. P. *J. Am. Chem. Soc.* **2000**, *122*, 4841−4842.
(13) Cordier, F.; Brutscher, B.; Marion, D. *J. Biomol. NMR* **1996**, *7*, 163−168.
(14) Reif, B.; Hennig, M.; Griesinger, C. *Science* **1997**, *276*, 1230−1233.
(15) Lundstrom, P.; Mulder, F. A. A.; Akke, M. *Proc. Natl. Acad. Sci. U.S.A.* **2005**, *102*, 16984−16989.
(16) Fruh, D.; Tolman, J. R.; Bodenhausen, G.; Zwahlen, C. *J. Am. Chem. Soc.* **2001**, *123*, 4810−4816.
(17) Muhandiram, D. R.; Yamazaki, T.; Sykes, B. D.; Kay, L. E. *J. Am. Chem. Soc.* **1995**, *117*, 11536−11544.
(18) Tjandra, N.; Szabo, A.; Bax, A. *J. Am. Chem. Soc.* **1996**, *118*, 6986−6991.
(19) Lipari, G.; Szabo, A. *J. Am. Chem. Soc.* **1982**, *104*, 4559−4570.

10.1021/ja072717t CCC: $37.00

parameters can also be used to obtain thermodynamic information about the system since in certain cases they can be simply related to entropy.[21−23] Relaxation rates of backbone nuclei provide structural information in the form of long-range orientational restraints of individual bonds relative to the rotational diffusion tensor, complementing short-range proton−proton NOE distances.[24]

In addition to their sensitivity to rapid picosecond−nanosecond motions, R_2 relaxation rates can also be affected by dynamics occurring on a microsecond−millisecond time scale (chemical exchange) and methods have recently emerged for studying these slower processes.[25,26] In many cases these exchange contributions to relaxation provide detailed information about the energy landscape that drives the exchange process as well as structural information about the states that participate in the exchange event.[27] On the other hand exchange contributions complicate interpretation of the relaxation rates in terms of picosecond−nanosecond dynamics parameters and care must be taken to ensure, for example, that robust measures of order parameters are obtained. In this context a particularly elegant set of experiments was developed by Palmer and co-workers[28] in which both transverse (η_{xy}) and longitudinal (η_z) $^1H-^{15}N$ dipole, ^{15}N chemical shift anisotropy (CSA) cross-correlated relaxation rates are measured and the ratio η_{xy}/η_z is used in place of ^{15}N R_2 rates to extract picosecond−nanosecond motional information. Unfortunately the extraction of accurate values of η_z is compromised by the fact that the magnetization of interest in this experiment decays more rapidly with increasing molecular weight, while the desired cross-correlation rate diminishes with size, leading to sensitivity issues. In addition, in experiments performed in our laboratory we have obtained η_{xy}/η_z ratios that were larger than expected, which we attribute to cross-relaxation between $^1H^N$ and proximal protons, leading to calculated negative values of exchange. Such negative values were observed even in perdeuterated molecules.

Herein, we describe an alternate approach for obtaining robust transverse relaxation rates "uncontaminated" by chemical exchange, based on measurements of longitudinal order, single quantum relaxation rates in the presence of either ^1H or ^{15}N spin-lock fields and multiple quantum $^1H-^{15}N$ relaxation rates measured when both ^1H and ^{15}N spin-locks are applied. The signal decay profiles measured in a set of four experiments are combined to isolate only contributions from $^1H-^{15}N$ dipolar relaxation. The utility of the methodology is illustrated both by simulation and by experiment, and it is shown that robust chemical exchange-free transverse relaxation rates can be obtained. Finally, an application involving the measurement of backbone order parameters in a partially folded folding intermediate of a redesigned apocytochrome b_{562} protein[29,30] is presented where ^{15}N R_2 values are severely affected by chemical exchange throughout all regions of the molecule.

Materials and Methods

Sample Preparation: U-[^{15}N,^2H] Ubiquitin was expressed with a cleavable His-tag and purified by standard methods,[31] and a 2.2 mM protein sample, 20 mM Na_3PO_4, 10 mM NaCl, 0.03% NaN_3, 90%/10% H_2O/D_2O, pH 5.5, was used for all studies. A second protein, U-[^{15}N,^2H]-protein L, was prepared as described;[32] the protein concentration was 2.7 mM in 50 mM Na_3PO_4, 20 μM EDTA, 0.05% NaN_3, 90%/10% H_2O/D_2O, pH 6.0. Starting from the sequence of redesigned apocytochrome b_{562}[30] additional mutations were made to generate a stabilized folding intermediate (W7D, L10G, L14G, V16G, I17G, I98G, Y101G, and Y105G), referred to in what follows as *PUF1**[33,34]. U-[^{15}N,^2H] *PUF1** was prepared as described previously[29,34] to produce a protein sample (2.5 mM) in 50 mM NaAc-^3D, 90%/10% H_2O/D_2O, pH 4.9.

NMR Spectroscopy: The four relaxation rates $R_{1\rho}(2H'_zN_z)$, $R_{1\rho}(2H_zN'_z)$, $R_{1\rho^2}(2H'_zN'_z)$, and $R_1(2H_zN_z)$ were measured for ubiquitin (298 K) and protein L (278 K) at static magnetic field strengths of 11.7 and 18.8 T (room-temperature probe heads), using pulse schemes illustrated in Figure 1. Relaxation delays between 2 and 35 ms were used for all experiments (same delays used for each rate measurement), along with ^1H and ^{15}N continuous wave CW spin-lock field strengths that varied between 11.5−13.7 kHz (^1H) and 1.8−2.1 kHz (^{15}N), depending on the sample. A total of 11 2D data sets were recorded for each relaxation rate determination, with net acquisition times of 4.5 h for each of the $R_{1\rho}(2H'_zN_z)$, $R_{1\rho}(2H_zN'_z)$, $R_{1\rho^2}(2H'_zN'_z)$ time series (i.e., 0.4 h/2D data set) and 3 h for the measurement of the longitudinal order decay, $R_1(2H_zN_z)$. Measurements of $R_{1\rho}(2H'_zN_z)$, $R_{1\rho}(2H_zN'_z)$, $R_{1\rho^2}(2H'_zN'_z)$, and $R_1(2H_zN_z)$ rates for *PUF1** were made at a static magnetic field of 14.1 T (288 K), using a cryogenically cooled probehead. ^1H and ^{15}N spin-lock fields of 12.7 kHz and 1.8 kHz were employed, respectively. A series of eight 2D data sets was collected for each type of rate measurement with relaxation time delays between 2 and 23.7 ms. The total acquisition time for each of the $R_{1\rho}(2H'_zN_z)$, $R_{1\rho}(2H_zN'_z)$, and $R_{1\rho^2}(2H'_zN'_z)$ series was 6.5 h (0.8 h/2D data set), while 4.3 h were required for the measurement of $R_1(2H_zN_z)$. Nitrogen relaxation dispersion profiles were recorded on *PUF1**, 14.1 T, using the pulse scheme of Tollinger et al.[35] that contains the relaxation compensation element described by Loria and co-workers.[36] Relaxation dispersion profiles were based on a series of 21 2D data sets where a variable number of ^{15}N 180° refocusing pulses are applied during a constant-time element of duration 36 ms. Field strengths, ν_{CPMG}, ranging from 55 to 1000 Hz were employed, where $\nu_{CPMG} = 1/(2\delta)$ and δ is the time between successive refocusing pulses. Dispersion data sets were analyzed as described in Korzhnev et al.[27]

Nitrogen R_1 and $R_{1\rho}$ relaxation rates along with steady-state $^1H-^{15}N$ NOE values[37] were obtained for the backbone amides of ubiquitin (298 K) and protein L (278 K) at static magnetic field strengths of 11.7 and 18.8 T, while for the backbone amides of *PUF1** relaxation

(20) Lipari, G.; Szabo, A. *J. Am. Chem. Soc.* **1982**, *104*, 4546−4559.
(21) Yang, D. W.; Kay, L. E. *J. Mol. Biol.* **1996**, *263*, 369−382.
(22) Akke, M.; Bruschweiler, R.; Palmer, A. G. *J. Am. Chem. Soc.* **1993**, *115*, 9832−9833.
(23) Lee, A. L.; Wand, A. J. *Nature* **2001**, *411*, 501−504.
(24) Tjandra, N.; Garrett, D. S.; Gronenborn, A. M.; Bax, A.; Clore, G. M. *Nat. Struct. Biol.* **1997**, *4*, 443−449.
(25) Palmer, A. G.; Kroenke, C. D.; Loria, J. P. *Methods Enzymol.* **2001**, *339*, 204−238.
(26) Palmer, A. G.; Grey, M. J.; Wang, C. Y. *Methods Enzymol.* **2005**, *394*, 430−465.
(27) Korzhnev, D. M.; Salvatella, X.; Vendruscolo, M.; Di Nardo, A. A.; Davidson, A. R.; Dobson, C. M.; Kay, L. E. *Nature* **2004**, *430*, 586−590.
(28) Kroenke, C. D.; Loria, J. P.; Lee, L. K.; Rance, M.; Palmer, A. G. *J. Am. Chem. Soc.* **1998**, *120*, 7905−7915.
(29) Feng, H. Q.; Zhou, Z.; Bai, Y. W. *Proc. Natl. Acad. Sci. U.S.A.* **2005**, *102*, 5026−5031.
(30) Chu, R.; Takei, J.; Knowlton, J. R.; Andrykovitch, M.; Pei, W. H.; Kajava, A. V.; Steinbach, P. J.; Ji, X. H.; Bai, Y. W. *J. Mol. Biol.* **2002**, *323*, 253−262.
(31) Distefano, D. L.; Wand, A. J. *Biochemistry* **1987**, *26*, 7272−7281.
(32) Scalley, M. L.; Yi, Q.; Gu, H. D.; McCormack, A.; Yates, J. R.; Baker, D. *Biochemistry* **1997**, *36*, 3373−3382.
(33) Feng, H. Q.; Takei, J.; Lipsitz, R.; Tjandra, N.; Bai, Y. W. *Biochemistry* **2003**, *42*, 12461−12465.
(34) Chu, R. A.; Pei, W. H.; Takei, J.; Bai, Y. W. *Biochemistry* **2002**, *41*, 7998−8003.
(35) Tollinger, M.; Skrynnikov, N. R.; Mulder, F. A. A.; Forman-Kay, J. D.; Kay, L. E. *J. Am. Chem. Soc.* **2001**, *123*, 11341−11352.
(36) Loria, J. P.; Rance, M.; Palmer, A. G. *J. Am. Chem. Soc.* **1999**, *121*, 2331−2332.
(37) Farrow, N. A.; Muhandiram, R.; Singer, A. U.; Pascal, S. M.; Kay, C. M.; Gish, G.; Shoelson, S. E.; Pawson, T.; Formankay, J. D.; Kay, L. E. *Biochemistry* **1994**, *33*, 5984−6003.

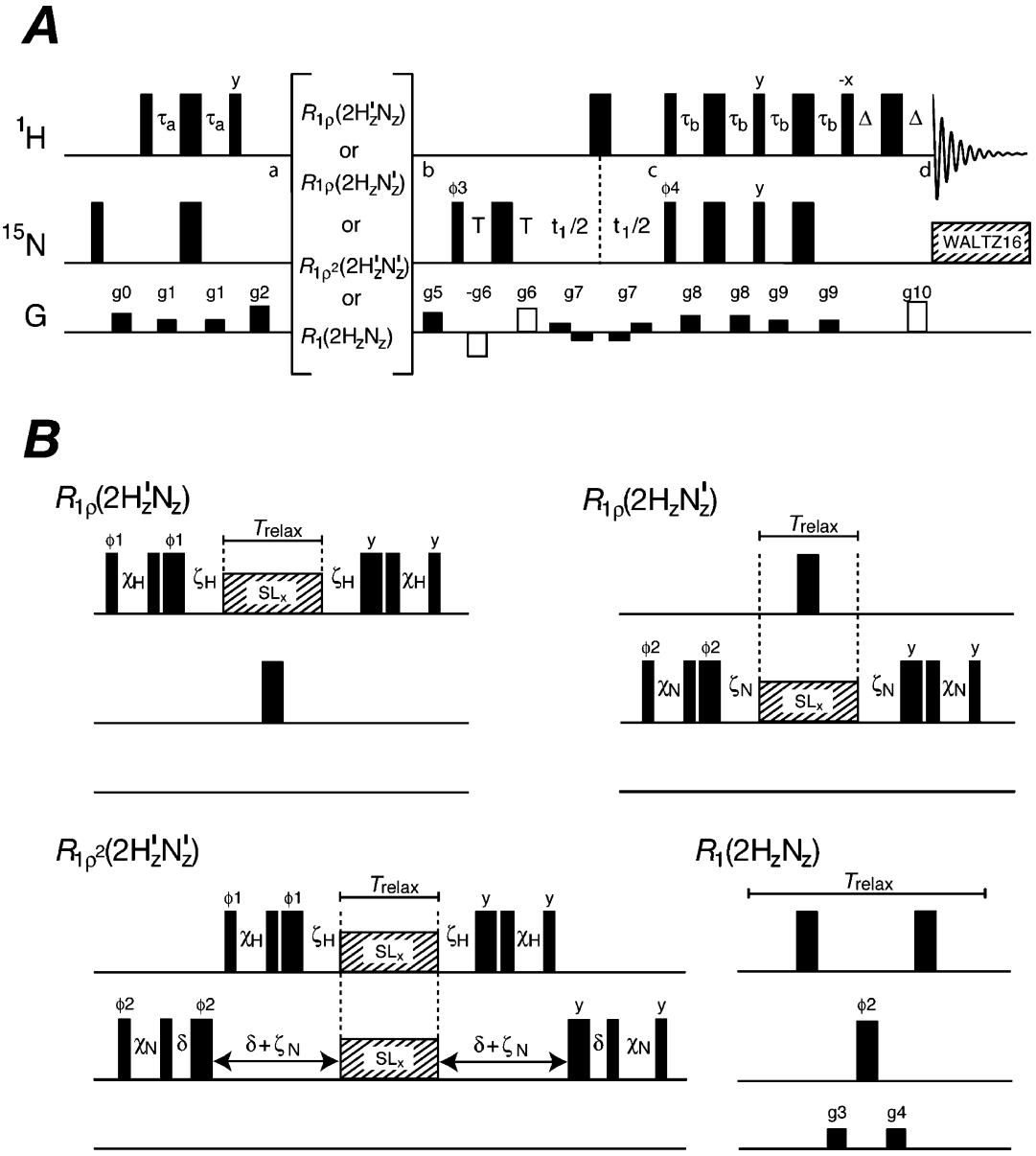

Figure 1. Pulse schemes for measurement of the four $^1H-^{15}N$ relaxation rates, $R_{1\rho}(2H'_zN_z)$, $R_{1\rho}(2H_zN'_z)$, $R_{1\rho^2}(2H'_zN'_z)$, and $R_1(2H_zN_z)$. One of the subsequences of part B is inserted into the square bracket of part A. The ^1H carrier is initially placed on water and subsequently positioned at 9.5 ppm between *a* and *b*. Typical ^1H and ^{15}N spin-lock fields ($\omega_{SL,A}$) are 13 and 2 kHz, respectively. All other pulses are applied at the highest possible power levels, with the exception of decoupling, where a 1.5 kHz WALTZ-16 field[53] is employed. The elements immediately flanking the spin-lock period are used to align magnetization along the effective field, as described in detail previously.[50] The delays used are as follows: $\tau_a = 2.25$ ms, $\tau_b = 2.68$ ms, $T = 2.25$ ms, $\Delta = 0.50$ ms, $\chi_A = 1/\omega_{SL,A} - 2/\omega_{1,A}$, $\zeta_A = 1/\omega_{1,A}$; δ is chosen to be sufficiently long so that ^1H alignment scheme can be inserted, and $\omega_{1,A}$ is the field strength (rad/s) used for high power pulses on spin A (^1H,^{15}N). Pulses without annotation are applied with *x*-phase. The phase cycles are as follows: $R_{1\rho}(2H'_zN_z)$ $\phi1 = 2(-y),2(y)$, $\phi3 = x,-x$, $\phi4 = x$, rec $= x,2(-x),x$; $R_{1\rho}(2H_zN'_z)$ $\phi2 = 2(-y),2(y)$, $\phi3 = x,-x$, $\phi4 = x$, rec $= x,2(-x),x$; $R_{1\rho^2}(2H'_zN'_z)$ $\phi1 = 2(-y),2(y)$, $\phi2 = -y,y$, $\phi3 = x$, $\phi4 = x$, rec $= x,2(-x),x$; $R_1(2H_zN_z)$ $\phi2 = x,-x$, $\phi3 = 2(x),2(-x)$, $\phi4 = x$, rec $= 2(x),2(-x)$; Quadrature detection in the indirect ^{15}N dimension is obtained by the enhanced sensitivity pulsed field gradient method,[49,54] where separate data sets are recorded for (g6, $\phi4$) and ($-$g6, $\phi4 + 180°$). The strength (G/cm) and duration (ms) of the gradients are as follows: g0, (8.0,1.0); g1, (4.0,0.7); g2, (10.0,1.0); g3, (2.0,0.13); g4, (7.5,0.17); g5, (15,1.0); g6, (15,1.25); g7, (0.5, $\tau_1/2$); g8, (8.0,1.2); g9, (4.0,1.2); g10, (29.45,0.125).

measurements were obtained at 11.7, 14.1, and 18.8 T. Relaxation delays between 10 ms and 1.4 s and between 2 and 100 ms were used to monitor the R_1 and $R_{1\rho}$ rates, respectively. The CW field strengths applied during the spin-lock period in the $R_{1\rho}$ experiments were very close to 1.9 kHz in all studies. Fine-power adjustments were used to calibrate the ^{15}N CW spin-lock field strength in $R_{1\rho}$ measurements of *PUF1**, so as to obtain identical spin-lock powers at all the static magnetic field strengths. The $^1H-^{15}N$ NOEs were determined from two spectra, with and without proton presaturation. The spectrum with presaturation was recorded with a prescan delay of 9 s followed by 6 s of proton saturation, while the spectrum without proton presaturation was recorded with a 15 s prescan delay. The corresponding total recording times were 4.5, 3, and 4.3 h for the $R_{1\rho}$, R_1, and NOE experiments, respectively for protein L and ubiquitin, while the total recording times were 9, 6, and 8.6 h for the $R_{1\rho}$, R_1, and NOE experiments for *PUF1**.

Data Processing: Data sets were processed with the NMRPipe program[38] and analyzed with UCSF Sparky.[39] Signal intensities were determined using the program FuDA[40] by fitting a mixed Gaussian/

(38) Delaglio, F.; Grzesiek, S.; Vuister, G. W.; Zhu, G.; Pfeifer, J.; Bax, A. *J. Biomol. NMR* **1995**, *6*, 277−293.
(39) Kneller, D. G.; Kuntz, I. D. *J. Cell. Biochem.* **1993**, 254−254.
(40) Kristensen, S. M.; Hansen, D. F. FuDA: A function and data fitting and analysis package (smk@kiku.dk), 2006.

Lorentzian line shape to each correlation and assuming a common line shape for a given cross-peak during a relaxation series (i.e., line shape and peak positions are independent of T_{relax}). Nitrogen R_1 and $R_{1\rho}$ relaxation rates were determined by fitting a single-exponential decay function [$I(T_{relax}) = A\exp(-RT_{relax})$] to the measured intensity vs T_{relax} profile. R_{dd} rates were quantified by fitting a single-exponential decay function of the form $A\exp(-2R_{\Sigma,\rho}T_{relax})$ to the time evolution of $I(2H'_zN_z) \times I(2H_zN'_z)/[I(2H'_zN'_z) \times I(2H_zN_z)]$ where $I(O_p)$ is the time-dependent intensity of the signal in experiments that measure the decay rate of O_p (see below). Uncertainties in relaxation rates were calculated using the covariance matrix method.[41]

Results and Discussion

Theoretical Aspects: We consider first a heteronuclear $^1H-^{15}N$ dipolar and scalar coupled spin system and focus on a number of coherences and magnetization modes that can be easily created and that will prove useful for isolating dipolar from non-dipolar contributions to relaxation. Our goal is to develop experiments that measure relaxation rates that can be combined in such a way as to eliminate all non-$^1H^N-^{15}N$ dipolar contributions to spin relaxation. In the discussion that follows we focus on longitudinal two-spin order, $2H_zN_z$, the transverse antiphase single quantum coherences, $2H_xN_z$ and $2H_zN_x$, and multiquantum coherence, $2H_xN_x$, where A_q is the q component of A magnetization. It is straightforward to show that their autorelaxation rates,[42−44] neglecting contributions from cross-correlated spin relaxation, are

$$R_1(2H_zN_z) = \frac{d_{HN}^2}{8}\Big(6J(\omega_N) + 6J(\omega_H)\Big) + c_N^2 J(\omega_N) + c_H^2\tilde{J}(\omega_H) + \lambda_N + \lambda_H \quad (1)$$

$$R_2(2H_xN_z) = \frac{d_{HN}^2}{8}\Big(4J(0) + J(\omega_H - \omega_N) + 3J(\omega_H) + 6J(\omega_H + \omega_N)\Big) + c_N^2 J(\omega_N) + \frac{c_H^2}{6}\Big(4\tilde{J}(0) + 3\tilde{J}(\omega_H)\Big) + \vartheta_H + \lambda_N + R_{ex}(H_x) \quad (2)$$

$$R_2(2H_zN_x) = \frac{d_{HN}^2}{8}\Big(4J(0) + J(\omega_H - \omega_N) + 3J(\omega_N) + 6J(\omega_H + \omega_N)\Big) + \frac{c_N^2}{6}\Big(4J(0) + 3J(\omega_N)\Big) + c_H^2\tilde{J}(\omega_H) + \vartheta_N + \lambda_H + R_{ex}(N_x) \quad (3)$$

$$R_2(2H_xN_x) = \frac{d_{HN}^2}{8}\Big(3J(\omega_N) + J(\omega_H - \omega_N) + 3J(\omega_H) + 6J(\omega_H + \omega_N)\Big) + \frac{c_N^2}{6}\Big(4J(0) + 3J(\omega_N)\Big) + \frac{c_H^2}{6}\Big(4\tilde{J}(0) + 3\tilde{J}(\omega_H)\Big) + \vartheta_H + \vartheta_N + R_{ex}(2H_xN_x) \quad (4)$$

where $d_{HN} = (\mu_0/4\pi)\hbar\gamma_H\gamma_N r_{HN}^{-3}$, $c_N = B_0\gamma_N\Delta\sigma_N/\sqrt{3}$, $c_H = B_0\gamma_H\Delta\sigma_H\sqrt{(1+\eta_H^2/3)}/3$, μ_0 is the permeability of free space, $\hbar$ is Planck's constant divided by 2π, γ_H and γ_N are the magnetogyric ratios of ^1H and ^{15}N, respectively, r_{HN} is the vibrationally averaged distance between ^1H and ^{15}N nuclei in the two-spin system, B_0 is the static magnetic field strength, $\Delta\sigma_N = \sigma_{||,N} - \sigma_{\perp,N}$, where $\sigma_{||,N}$ and $\sigma_{\perp,N}$ are the parallel and transverse principal components of the axially symmetric nitrogen chemical shift anisotropy (CSA) tensor, respectively, $\Delta\sigma_H = \sigma_{11,H} - (\sigma_{22,H} + \sigma_{33,H})/2$ (shift anisotropy) and $\eta_H = (\sigma_{11,H} - \sigma_{22,H})/\sigma_{33,H}$ (reduced asymmetry), where $\sigma_{11,H}$, $\sigma_{22,H}$, and $\sigma_{33,H}$ are the principal components of the proton CSA tensor.[45] The power spectral density function, $J(\omega)$, describes the frequency distribution of the stochastic motions that modulate both the $^1H-^{15}N$ dipole−dipole and the ^{15}N CSA interactions. A single spectral density function is used, to a good approximation, since the $^1H-^{15}N$ vector and the symmetry axis of the (assumed) axially symmetric ^{15}N CSA tensor are nearly collinear (≈20°) for an amide group.[45] The power spectral density function, $\tilde{J}(\omega)$, describes the modulation of the asymmetric ^1H CSA interaction. The contributions to the longitudinal relaxation of the ^1H (^{15}N) spin from interactions with external spins are given by λ_H (λ_N), while ϑ_H and ϑ_N are additions to ^1H and ^{15}N transverse relaxation rates, respectively, that result from interactions with proximal external spins and from other magnetization leaking mechanisms such as exchange with the solvent, for example. Finally, $R_{ex}(H_x)$, $R_{ex}(N_x)$, and $R_{ex}(2H_xN_x)$ are the contributions to the H_x, N_x, and $2H_xN_x$ relaxation rates that originate from fluctuations of the Zeeman Hamiltonian (the chemical shift) caused by chemical exchange processes.

Central to the present discussion is the linear combination of rates,

$$R_\Sigma = \frac{1}{2}[R_2(2H_xN_z) + R_2(2H_zN_x) - R_2(2H_xN_x) - R_1(2H_zN_z)] \quad (5.1)$$

that we express as

$$R_\Sigma = R_{dd} + \Delta R_{ex} \quad (5.2)$$

where from eqs 1−4,

$$R_{dd} = \frac{d_{HN}^2}{8}\Big(4J(0) + \frac{1}{2}J(\omega_H - \omega_N) - 3J(\omega_N) - 3J(\omega_H) + 3J(\omega_H + \omega_N)\Big) \quad (6.1)$$

$$\Delta R_{ex} = \frac{1}{2}[R_{ex}(H_x) + R_{ex}(N_x) - R_{ex}(2H_xN_x)] \quad (6.2)$$

Interestingly, for chemical exchange processes in the fast exchange regime $\Delta R_{ex} = 0$ (so long as the double- and zero-quantum components of $2H_xN_x$ are interchanged during the measurement)[46] so that $R_\Sigma = R_{dd}$ and in this limit R_Σ depends only on the $^1H-^{15}N$ dipolar contribution. By contrast, $\Delta R_{ex} \neq 0$ outside of this regime. For example, consider the simple case of slow exchange between two sites, A and B. Then the exchange contribution, R_{ex}, to the relaxation of each of the coherences H_x, N_x, and $2H_xN_x$ that derive from site A is the lifetime of that site, τ_A^{-1}, so that $R_{ex}(H_x) + R_{ex}(N_x) = 2\tau_A^{-1} \neq \tau_A^{-1} = R_{ex}(2H_xN_x)$.

The above results establish that in general R_Σ is not exchange-free. However, it is possible to construct a set of experiments for which relaxation rates are essentially independent of

(41) Press, W. H.; Flannery, B. P.; Teukolsky, S. A.; Vetterling, W. T. *Nummerical Recipes in C*; Cambridge University Press: Cambridge, 1988.
(42) Abragam, A. *Principles of nuclear magnetism*; Clerendon Press: Oxford, 1961.
(43) Peng, J. W.; Wagner, G. *J. Magn. Reson.* **1992**, *98*, 308−332.
(44) Allard, P.; Helgstrand, M.; Hard, T. *J. Magn. Reson.* **1998**, *134*, 7−16.
(45) Cornilescu, G.; Bax, A. *J. Am. Chem. Soc.* **2000**, *122*, 10143−10154.
(46) Kloiber, K.; Konrat, R. *J. Biomol. NMR* **2000**, *18*, 33−42.

exchange by exploiting the fact that application of a continuous wave radio frequency (RF) spin-lock field partially quenches transverse relaxation caused by chemical exchange processes slower than the field strength of the spin-locking pulse.[47] Thus, by measuring relaxation rates in the presence of strong spin-lock fields that quench exchange processes in the slow to intermediate regime, while exchange in the fast regime cancels naturally from the combination considered in R_Σ (eq 5.1), $R_\Sigma \approx R_{dd}$ for all exchange processes, as shown below.

Consider the relaxation of the analogous elements to the four listed in eqs 1−4, but where ^{1}H and ^{15}N magnetization components are spin-locked along their effective fields. Thus, in the case of proton magnetization the effective field is along the axis defined by $\hat{z}'_H = \cos(\theta_H)\,\hat{z} + \sin(\theta_H)\,\hat{x}$, where $\hat{x}$ and $\hat{z}$ are direction vectors in the conventional ^{1}H rotating frame, $\tan(\theta_H) = \omega_{SL,H}/\Omega_H$, $\omega_{SL,H}$ is the field strength (rad/s) of the ^{1}H spin-lock field that is applied along the *x*-axis of the rotating frame, and Ω_H is the offset (rad/s) of the ^{1}H spin from the ^{1}H RF carrier. An analogous set of equations applies to nitrogen magnetization as well. In what follows below magnetization that is spin-locked along its effective field ($\hat{z}'_H$, $\hat{z}'_N$ for ^{1}H and ^{15}N, respectively) is denoted with "primes", so that $A'_z = A_z \cos\theta_A + A_x \sin\theta_A$ refers to magnetization spin-locked along $\hat{z}'_A$ (A = ^{1}H, ^{15}N), where the "unprimed" operators indicate magnetization in the rotating (unlocked) frame. Thus $R_{1\rho}(2H'_zN_z)$ refers to the relaxation rate measured in the presence of a strong ^{1}H spin-lock field, where $R_2(2H_xN_z)$ is the analogous rate in the free precession limit. Similarly $R_{1\rho^2}(2H'_zN'_z)$ is measured in the presence of simultaneous ^{1}H and ^{15}N spin-lock fields. Assuming that $\omega_{eff,A}\tau_R \ll 1$, $\omega_{eff,A} \ll \omega_N, \omega_H$, where $\omega_{eff,A} = \sqrt{\omega_{SL,A}^2 + \Omega_A^2}$ and τ_R is the correlation time of the assumed isotropic molecular tumbling, the autorelaxation rates in the tilted rotating frames are[43,48]

$$R_{1\rho}(2H'_zN_z) = R_2(2H_xN_z)\sin^2\theta_H + R_1(2H_zN_z)\cos^2\theta_H \quad (7)$$

$$R_{1\rho}(2H_zN'_z) = R_2(2H_zN_x)\sin^2\theta_N + R_1(2H_zN_z)\cos^2\theta_N \quad (8)$$

$$R_{1\rho^2}(2H'_zN'_z) = R_2(2H_xN_x)\sin^2\theta_H\sin^2\theta_N + R_2(2H_xN_z)\sin^2\theta_H\cos^2\theta_N + R_2(2H_zN_x)\cos^2\theta_H\sin^2\theta_N + R_1(2H_zN_z)\cos^2\theta_H\cos^2\theta_N \quad (9)$$

where the expressions for R_2 are as listed in eqs 1−4. It is understood, however, that the expressions for the R_{ex} rates must be modified from those that apply in the laboratory frame to take into account the spin-lock field(s), $\omega_{SL,A}$. A linear combination of the four rates is constructed, analogous to what was done above,

$$R_{\Sigma,\rho} = \tfrac{1}{2}[\underbrace{R_{1\rho}(2H'_zN_z) + R_{1\rho}(2H_zN'_z)}_{R_{SQ}} - \underbrace{(R_{1\rho^2}(2H'_zN'_z) + R_1(2H_zN_z))}_{R_{MQ,ZQ}}] \quad (10)$$

and from eqs 7−9

$$R_{\Sigma,\rho} = \sin^2\theta_H\sin^2\theta_N(R_{dd} + \Delta R'_{ex}) \quad (11.1)$$

independent of contributions from CSA. We will show below, through detailed simulations, that $R_{\Sigma,\rho}$ is to an excellent approximation also insensitive to chemical exchange over the complete exchange regime (i.e., $\Delta R'_{ex} \approx 0$, for exchange processes ranging from slow to fast, where the (′) indicates that these are exchange contributions in the presence of spin-lock fields). Simulations that include cross-relaxation with external proton spins also establish that $R_{\Sigma,\rho}$ is very little affected by external protons so long as levels of protein deuteration exceed approximately 50% (see below), so that to an excellent approximation

$$R_{\Sigma,\rho} \approx \sin^2\theta_H\sin^2\theta_N R_{dd} \quad (11.2)$$

The $R_{\Sigma,\rho}$ rate can be readily obtained from four NMR relaxation experiments, described below, that quantify either the single quantum rates, $R_{1\rho}(2H'_zN_z)$ and $R_{1\rho}(2H_zN'_z)$, or the decay of the multiquantum, $R_{1\rho^2}(2H'_zN'_z)$ and the two-spin longitudinal order, $R_1(2H_zN_z)$, states.

Experimental Implementation: Figure 1A illustrates the pulse schemes that have been derived for the measurement of $R_{1\rho}(2H'_zN_z)$, $R_{1\rho}(2H_zN'_z)$, $R_{1\rho^2}(2H'_zN'_z)$, and $R_1(2H_zN_z)$. The experiments follow closely on the basic enhanced-sensitivity ^{1}H−^{15}N HSQC sequence,[49] with an additional element, Figure 1B, inserted at point *a* when the density operator of interest is proportional to $2H_zN_z$. The pulse/delay element of Figure 1B immediately preceding and following the spin-lock period of duration T_{relax} ensures that each magnetization component is locked along its effective field during application of the spin-lock and subsequently returned to the *z*-axis at the completion of the relaxation element. The mechanics of the alignment scheme are described in detail elsewhere.[50] ^{1}H/^{15}N 180° pulses applied during the T_{relax} periods that quantify $R_{1\rho}(2H'_zN_z)$, $R_{1\rho}(2H_zN'_z)$, and $R_1(2H_zN_z)$ effectively suppress cross-correlation relaxation interference between the ^{1}H−^{15}N dipole and either ^{1}H or ^{15}N CSA interactions.[51,52] At the conclusion of the spin-lock element, ^{15}N chemical shift is recorded (between *b* and *c*) and magnetization is subsequently transferred back to ^{1}H (*c* to *d*) for detection. Thus, correlations are observed at (Ω_N,Ω_H) with intensities proportional to $\exp(-T_{relax}R)$, where $R = R_{1\rho}(2H'_zN_z)$, $R_{1\rho}(2H_zN'_z)$, $R_{1\rho^2}(2H'_zN'_z)$, or $R_1(2H_zN_z)$, depending on the experiment.

Validation from Simulations: In order to establish that $R_{\Sigma,\rho}$ is sensitive only to the intraresidue ^{1}H−^{15}N dipolar interaction, as implied by eq 11.2, we have turned to simulations. Specifically, we wish to evaluate how effectively the experimental scheme proposed in Figure 1 suppresses chemical exchange and to what extent cross-relaxation with external spins affects the measured R_{dd} rate. The details of the simulations are given in the Supporting Information. Briefly, we have followed the formalism of Allard and co-workers,[44,55,56] who have derived a master equation for the evolution of a two-spin heteronuclear spin system, and we have modified their equations to include chemical exchange, ^{1}H CSA, and for some applications a third

(47) Deverell, C.; Morgan, R. E.; Strange, J. H. *Mol. Phys.* **1970**, *18*, 553−559.
(48) Korzhnev, D. M.; Billeter, M.; Arseniev, A. S.; Orekhov, V. Y. *Prog. Nucl. Magn. Reson. Spectrosc.* **2001**, *38*, 197−266.
(49) Kay, L. E.; Keifer, P.; Saarinen, T. *J. Am. Chem. Soc.* **1992**, *114*, 10663−10665.
(50) Hansen, D. F.; Kay, L. E. *J. Biomol. NMR* **2007**, *37*, 245−255.
(51) Kay, L. E.; Nicholson, L. K.; Delaglio, F.; Bax, A.; Torchia, D. A. *J. Magn. Reson.* **1992**, *97*, 359−375.
(52) Palmer, A. G.; Skelton, N. J.; Chazin, W. J.; Wright, P. E.; Rance, M. *Mol. Phys.* **1992**, *75*, 699−711.
(53) Shaka, A. J.; Keeler, J.; Frenkiel, T.; Freeman, R. *J. Magn. Reson.* **1983**, *52*, 335−338.

spin (external proton). Chemical exchange has been considered using a simple two-site exchange model,

$$A \underset{k_{BA}}{\overset{k_{AB}}{\rightleftharpoons}} B$$

where the population of the minor state B, p_B, and $k_{ex} = k_{AB} + k_{BA}$ are allowed to vary. The simulated rates, $R_{SQ} = R_{1\rho}(2H'_zN_z) + R_{1\rho}(2H_zN'_z)$ and $R_{MQ,ZO} = R_{1\rho^2}(2H'_zN'_z) + R_1(2H_zN_z)$ (see eq 10) are obtained by fitting a two-parameter single-exponential decay function, $A\exp(-T_{relax}R)$, to $A_{SQ}(T_{relax}) = I(2H'_zN_z)I(2H_zN'_z)$ and $A_{MQ,ZO}(T_{relax}) = I(2H'_zN'_z)I(2H_zN_z)$, respectively, where $I(O_p)$ is the measured time dependence of the intensity of $O_p \in \{2H'_zN_z, 2H_zN'_z, 2H'_zN'_z, 2H_zN_z\}$. The $R_{\Sigma,\rho}$ rate is, in turn, obtained by fitting a two-parameter single-exponential function, $\alpha\exp(-2R_{\Sigma,\rho}T_{relax})$, to the ratio, $\beta = A_{SQ}(T_{relax})/A_{MQ,ZO}(T_{relax})$, noting that

$$\frac{-1}{2T_{relax}}(\ln\beta - \ln\alpha) = R_{\Sigma,\rho}$$

with $R_{dd} + \Delta R'_{ex}$ subsequently calculated from eq 11.1. Figure 2A plots R_{SQ} (green), $R_{MQ,ZO}$ (red), and $R_{dd} + \Delta R'_{ex}$ (blue) as a function of p_B (1−10%) and k_{ex} for ^1H and ^{15}N chemical shift differences between states A and B of 550 and 600 Hz, respectively. These shift differences are on the very high end of what is usually observed[27] and thus provide a rigorous test of the method. The calculated $R_{dd} + \Delta R'_{ex}$ is expanded in Figure 2B and compared with the expected value of R_{dd} that is calculated directly from eqs 6.1 and 11.2 based on the input parameters (i.e., the absence of exchange, $\Delta R'_{ex} = 0$; dashed line). The simulated values of $R_{dd} + \Delta R'_{ex}$ can be either below or above the dashed line, depending on the ^{15}N offset, and do not coincide with the dashed line because of residual cross-correlation effects that are incompletely suppressed by the schemes described in Figure 1. Simulations like those in Figure 2 establish that the effects of exchange are eliminated to better than 99% over a wide range of exchange parameters.

In addition to quantifying the potential contributions from chemical exchange we were also interested in examining how proton spins proximal to the amide group in question might influence extracted R_{dd} rates. Here we have considered a three-spin spin system by including an additional proton, H_{eff}, located at a distance of r_{eff} from the amide proton spin, where

$$r_{eff} = \left(\sum_i r_{H-Hi}^{-6}\right)^{-1/6}$$

with the summation over all protons, H_i, in the protein excluding the amide proton in question. The evolution of the spin system has been calculated following a simulation protocol that is summarized in the Supporting Information. Calculations have been performed for proteins labeled in a number of ways, including a perdeuterated molecule, one with 50% random deuteration, and a fully protonated protein, as described below. Chemical exchange has also been included using the same parameters as those used in the simulations of Figure 2, but with a fixed population of the minor state of 2% along with k_{ex} = 10 000 s^{-1}, corresponding to the value of the exchange rate that gives the maximum contribution to the individual relaxation times for the chemical shift differences considered.

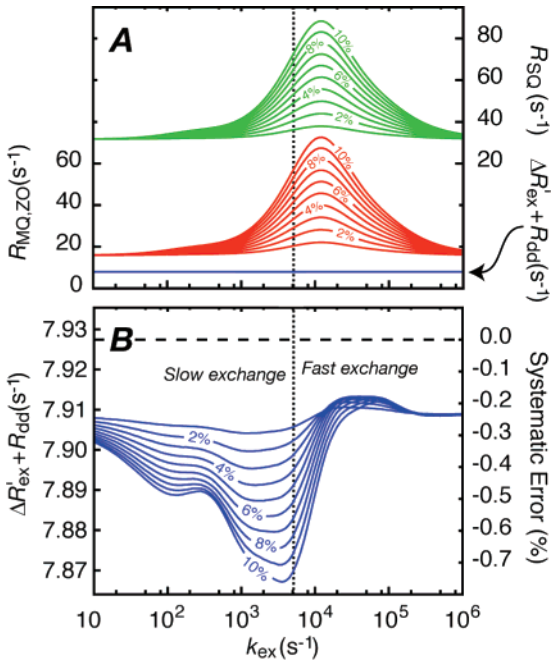

Figure 2. (A) $R_{SQ} = R_{1\rho}(2H'_zN_z) + R_{1\rho}(2H_zN'_z)$ (green), $R_{MQ,ZO} = R_{1\rho^2}(2H'_zN'_z) + R_1(2H_zN_z)$ (red), and $R_{dd} + \Delta R'_{ex}$ (blue) relaxation rates (14.1 T) vs exchange rate, k_{ex}, simulated for an isolated $^1H-^{15}N$ spin system in a protein. A correlation time of 10 ns and motion described by a model-free spectral density function[20] with $S^2 = 0.8$ and $\tau_e = 100$ ps have been assumed. Furthermore, leaking factors of $\vartheta_H = 10$ s^{-1} and $\lambda_H = 1$ s^{-1} (eq 1−4) were included to account, to first order, for external spins. All relaxation interactions and the effects of chemical exchange (assumed two-site) were included using the master equation of Allard and co-workers,[44,55,56] as described in the Supporting Information. The relative population of the minor site is indicated (from 1 to 10%). Chemical shift differences between exchanging sites of 550 and 600 Hz were assumed for ^1H and ^{15}N, respectively. (B) Expanded view of $R_{dd} + \Delta R'_{ex}$, showing that exchange introduces errors of less than 0.7%. The horizontal dashed line corresponds to the value of R_{dd} that is calculated directly from the input parameters in the simulation, 7.927 s^{-1} (eqs 6.2 and 11.1, $\Delta R'_{ex} = 0$). The dotted, vertical line is drawn at $k_{ex} = \sqrt{\Delta\omega_H^2 + \Delta\omega_N^2} = 5114$ s^{-1}, to delineate in a qualitative way the break between slow ($k_{ex} < \Delta\omega$) and fast ($k_{ex} > \Delta\omega$) exchange.

Figure 3 displays the systematic errors in R_{dd} as a function of r_{eff} that are calculated from simulations of a perdeuterated protein (A), a 50% random fractionally deuterated protein (B), and a fully protonated protein (C). In all cases it is assumed that the amide positions are completely protonated. Correlation times of 5 (red), 10 (green), and 15 ns (blue) are considered. Also indicated (insets) are the r_{eff} distance profiles that are calculated on the basis of high-resolution structures of a number of proteins and the labeling patterns considered. Curves are drawn only for distances that are observed in proteins and depicted in the insets, with continuous lines for $r_{eff} \geq r_o = 2.15$ Å (A), 1.94 Å (B), and 1.72 Å (C) and broken lines for $r_{eff} < r_o$; values of r_o are chosen such that for 98% of the $^1H-^{15}N$ spin-systems $r_o \leq r_{eff}$. The dashed black vertical lines denote the shortest distances observed in the set of proteins considered. The arrowheads shown on the ordinate axes indicate the upper error bounds for 98% of the $^1H-^{15}N$ spin systems (i.e., errors for $r_{eff} = r_o$).

The influence of external protons on the measured values of R_{dd} depends on the relaxation time points, T_{relax}, used in the

(54) Schleucher, J.; Sattler, M.; Griesinger, C. *Angew. Chem., Int. Ed.* **1993**, *32*, 1489−1491.
(55) Allard, P.; Helgstrand, M.; Hard, T. *J. Magn. Reson.* **1997**, *129*, 19−29.
(56) Helgstrand, M.; Hard, T.; Allard, P. *J. Biomol. NMR* **2000**, *18*, 49−63.

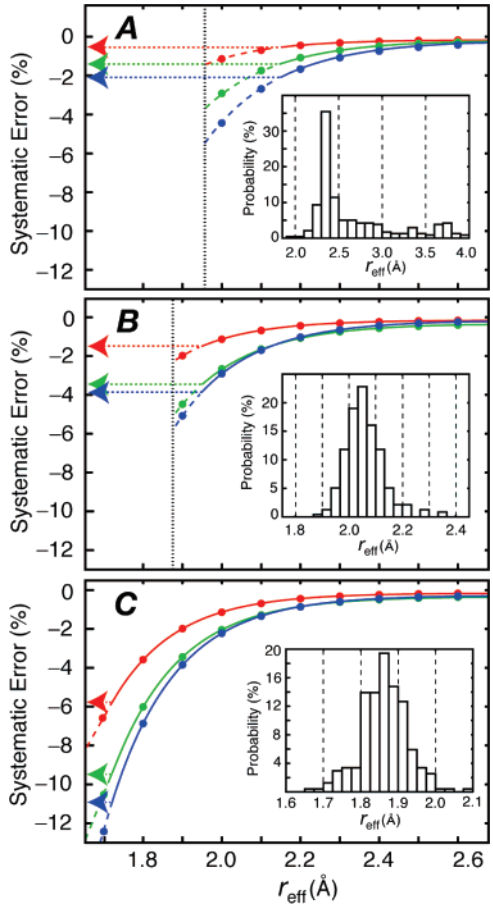

Figure 3. Systematic errors in the derived R_{dd} rates caused by external proton spins that are dipolar coupled to the amide proton in question in the case of a perdeuterated, amide protonated protein (A), a 50% random fractionally deuterated protein (B), and a fully protonated protein (C). Simulations were carried out for proteins with overall rotational correlation times of 5 ns (red), 10 ns (green), and 15 ns (blue), while the insets show the distribution of $r_{eff} = (\sum r_{H-Hi}^{-6})^{-1/6}$ for each of the labeling patterns considered. The distributions were calculated using coordinates of protein L (PDB: 1HZ6[57]), human ubiquitin (PDB: 1D3Z[58]), and cytochrome b_{562} (PDB: 256B[59]). For protein L and cytochrome b_{562} two molecules are present in the asymmetric unit and the average effective distances obtained for the two molecules were used. Ten NMR structures were present in the structure file of human ubiquitin, and the effective distances are the average over the ensemble of the ten structures. Effective distances were calculated in the case of 50% random fractional deuteration as the average of 1000 runs where 50% randomly selected protons were substituted by deuterons in each run. The arrowheads indicate the 98% confidence levels, as defined in the text. The vertical dashed lines delineate the lower distance limits obtained from the distance distributions in the insets. Details of the simulations used to calculate the errors are given in the text and in the Supporting Information. Leaking terms ϑ_H and λ_H (eq 1−4) were derived solely from the interactions with the external proton spin.

experiments. Typically the delays used to measure the relaxation of all four elements $\{2H'_zN_z, 2H_zN'_z, 2H'_zN'_z, 2H_zN_z\}$ are set the same (see below), with max(T_{relax}) adjusted so that the fastest relaxing coherence ($2H'_zN_z$) has decayed to approximately 50% of its initial value or max(T_{relax}) = 35 ms, whatever is shortest. In general we use an upper bound of 35 ms to minimize sample heating and dipolar contributions from neighboring spins in experiments, and this has been used in the simulations as well. Values of max(T_{relax}) vary of course with the correlation time of the protein, the overall level of deuteration, and r_{eff}. For example, using eqs 1−4 along with a simple model-free formulation for the spectral density function and values of 10 ns for the overall tumbling time, $S^2 = 0.8$, $\tau_e = 100$ ps, values of 46, 30, and 22 ms are calculated for 50% reduction in signal intensities of $2H'_zN_z$ for perdeuterated, 50% randomly deuterated, and fully protonated proteins, respectively (corresponding to T_2 values of 66, 43, and 32 ms). In the simulations presented we have used average values of r_{eff} of 2.350, 2.050, and 1.875 Å to calculate max(T_{relax}) for the three classes of proteins based on distributions of distances shown in the insets to Figure 3.

Systematic errors that would be expected in R_{dd} measurements have been calculated on a per-residue basis for protein L, ubiquitin, and cytochrome b_{562} for a number of different labeling patterns, Figure 4. Here we have assumed a correlation time of 10 ns for each protein and have calculated per-residue r_{eff} values based on high-resolution structures of the proteins, as described above. In cases where deuteration levels of at least 50% are employed, errors less than ∼4% are obtained. The largest errors are generally noted in loop regions. Although we have assumed constant dynamics parameters throughout each protein in the simulations ($S^2 = 0.8$, $\tau_e = 100$ ps) we would expect in general that there would be increased dynamics in the loop regions that would, in fact, decrease the errors (since $^1H-^1H$ cross relaxation effects will diminish).

It is clear that even for 50% fractionally deuterated proteins the level of systematic error is tolerable, although error levels are, in our view, unacceptably high for applications involving fully protonated molecules. In this regard it is of interest to note that external protons also introduce systematic errors in measurements of ^{15}N R_2 values. In particular, for fully protonated molecules contributions to ^{15}N R_2 rates on the order of 2−3% are estimated (14.1 T).

Finally, although we recommend recording spectra on highly deuterated proteins when possible, the simulations of Figures 3 and 4 indicate that the methodology is tolerant of a significant level of protonation. With this in mind we have also examined whether Hartmann−Hahn magnetization transfer[60,61] during the proton spin-lock element becomes an issue in these cases. In principle, such transfer becomes possible when two nuclei approach the strong-coupling condition during the application of a spin-lock field, and the transfer of magnetization between homonuclear spins I and S due to such mixing is given by[60−62]

$$I'_z \xrightarrow{\text{Isotropic mixing}} a_{II}(t_{mix})\, I'_z + a_{IS}(t_{mix})\, S'_z \qquad (12.1)$$

where

$$a_{IS}(t_{mix}) = \sin^2\phi \sin^2(q t_{mix}) \qquad (12.2)$$

$$a_{II}(t_{mix}) = 1 - a_{IS}(t_{mix}) \qquad (12.3)$$

$$q = \sqrt{(\Omega_{I,eff} - \Omega_{S,eff})^2 + (\pi J_{IS} \sin\theta_I \sin\theta_S)^2} \qquad (12.4)$$

$$\tan\phi = \frac{\pi J_{IS} \sin\theta_I \sin\theta_S}{\Omega_{I,eff} - \Omega_{S,eff}} \qquad (12.5)$$

$$\Omega_{I,eff} = \sqrt{\Omega_I^2 + \omega_{SL,I}^2} \text{ and } \Omega_{S,eff} = \sqrt{\Omega_S^2 + \omega_{SL,S}^2} \qquad (12.6)$$

and t_{mix} is the mixing time. In principle Hartmann−Hahn mixing between intraresidue amide and alpha protons is possible in experiments that quantify $R_{1\rho}(2H'_zN_z)$ and $R_{1\rho^2}(2H'_zN'_z)$ since a strong ^1H spin-lock field is employed. Such mixing could occur when the absolute offset of the amide proton approaches that of the alpha proton, and in order to minimize such effects, therefore, the ^1H carrier is moved to 9.5 ppm during the ^1H

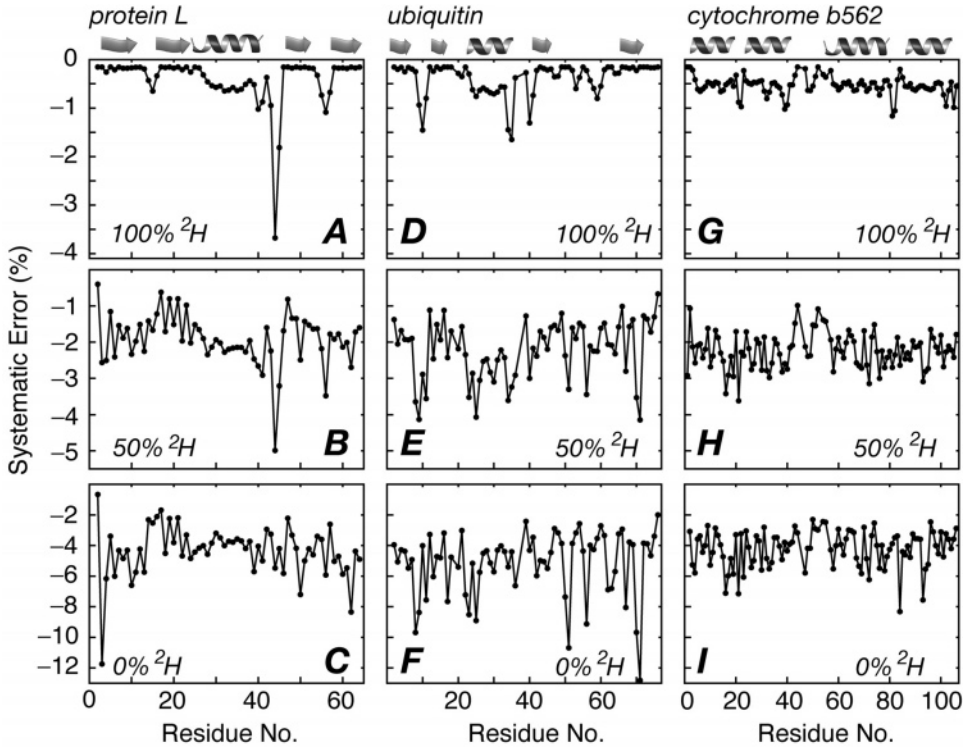

Figure 4. Systematic errors in calculated R_{dd} rates from dipolar relaxation involving remote protons. All calculations assumed protein tumbling times of 10 ns and measurements at a field strength of 14.1 T. (A−C) protein L (PDB: 1HZ6[57]), (D−F) human ubiquitin (PDB: 1D3Z[58]), (G−I) cytochrome b_{562} (PDB: 256B[59]). Proteins are deuterated at all positions with the exception of the amide sites (A, D, G), 50% randomly deuterated (B, E, H), or fully protonated (C, F, I). Effective distances, r_{eff}, for each amide proton in the three proteins were calculated as described in the text and in the legend to Figure 3 and converted into the systematic errors in R_{dd} according to Figure 3. Secondary structure elements for the three proteins are shown at the top. Residues showing large changes in error from 50% to 0% ^2H have amide protons that are within short distances of aliphatic spins, while amide protons from residues with larger than average errors in the 100% ^2H case are close to other amides.

spin-lock period. One particularly bad case is when the amide proton resonates far upfield, as is the case for Ile 36 in human ubiquitin, where the chemical shift of the amide proton is at 6.17 ppm and the alpha proton is at 4.45 ppm.[63] Here the isotropic mixing transfer, $a_{IS}(t_{mix})$, is up to 8% (4%) of the initial magnetization if the ^1H carrier is placed at 4.8 ppm, at a static magnetic field strength of 11.7 T (14.1 T), using a 13 kHz spin-lock field strength, and assuming a scalar coupling constant of 10 Hz between the alpha and amide protons. However, less than 0.1% of the initial magnetization is transferred when the ^1H carrier is positioned at 9.5 ppm.

Experimental Verification: In order to establish that accurate values of R_{dd} are obtained using the pulse schemes of Figure 1 we have compared experimentally determined values of the spectral density evaluated at zero frequency, $J(0)$, obtained from "standard" ^{15}N $R_{1\rho}$, R_1, and NOE measurements[43,64] with those calculated where $R_{1\rho}$ values are replaced by R_{dd} for a pair of proteins. Specifically, $J(0)$ has been obtained on a per-residue basis by mapping[43,65−67] the six experimentally measured values, $\{^{15}N\ R_1, ^{15}N\ R_{1\rho}, ^1H-^{15}N\ NOE\}_{11.7T}$ and $\{^{15}N\ R_1, ^{15}N\ R_{1\rho}, ^1H-^{15}N\ NOE\}_{18.8T}$, obtained at a pair of magnetic fields, onto $\{J(0), J(\omega_{N,11.7T}), J(\omega_{N,18.8T}), J(0.87\omega_{H,11.7T}), J(0.87\omega_{H,18.8T}), R_{ex}\}$, where R_{ex} is assumed to be proportional to B_0^2.[68] In a similar manner, $J(0)$ is obtained by mapping $\{^{15}N\ R_1, ^1H-^{15}N\ R_{dd}, ^1H-^{15}N\ NOE\}_{18.8T}$, *measured at a single field*, onto $\{J(0), J(\omega_{N,18.8T}), J(0.87\omega_{H,18.8T})\}$ by making use of the relation

$$R_{dd} = \frac{d_{HN}^2}{8}\left(4J(0) - 3J(\omega_N) + 0.845J(0.87\omega_H)\right) \quad (13)$$

that follows directly from $J(\epsilon\omega_H) \approx (0.87/\epsilon)^2\, J(0.87\ \omega_H)$, when $\omega_H\tau_C \gg 1$ and $\epsilon \approx 1$.[65] Note that R_{dd} values are expected to be independent of R_{ex} and there is no *a priori* reason to include an exchange term in this case. Figure 5A, C show the correlations between $J(0)$ values obtained using the two approaches for perdeuterated samples of protein L (A; 278 K, correlation time of approximately 8 ns) and ubiquitin (C; 298 K, correlation time of approximately 4.5 ns). The excellent agreement between $J(0)$ values calculated with the different methods is clear, establishing that the R_{dd} measurements are robust and independent of R_{ex}. Interestingly, nonzero R_{ex} values are obtained for many of the residues in both proteins based on analyses that involve ^{15}N $R_{1\rho}$ values, and indeed if such contributions are neglected the correlation between $J(0)$ values generated via the two methods shows a decided offset, particularly at low temperatures. Thus,

(57) O'Neill, J. W.; Kim, D. E.; Baker, D.; Zhang, K. Y. J., *Acta Crystallogr., Sect D* **2001**, *57*, 480−487.
(58) Cornilescu, G.; Marquardt, J. L.; Ottiger, M.; Bax, A. *J. Am. Chem. Soc.* **1998**, *120*, 6836−6837.
(59) Lederer, F.; Glatigny, A.; Bethge, P. H.; Bellamy, H. D.; Mathews, F. S. *J. Mol. Biol.* **1981**, *148*, 427−448.
(60) Hartmann, S. R.; Hahn, E. L. *Phys. Rev.* **1962**, *128*, 2042−2053.
(61) Muller, L.; Ernst, R. R. *Mol. Phys.* **1979**, *38*, 963−992.
(62) Cavanagh, J.; Fairbrother, W. J.; Palmer, A. G.; Skelton, N. J. *Protein NMR spectroscopy, principles and practise*; Academic Press: San Diego, 1996.
(63) Weber, P. L.; Brown, S. C.; Mueller, L. *Biochemistry* **1987**, *26*, 7282−7290.
(64) Kay, L. E.; Marion, D.; Bax, A. *J. Magn. Reson.* **1989**, *84*, 72−84.
(65) Farrow, N. A.; Zhang, O. W.; Szabo, A.; Torchia, D. A.; Kay, L. E. *J. Biomol. NMR* **1995**, *6*, 153−162.
(66) Ishima, R.; Nagayama, K. *Biochemistry* **1995**, *34*, 3162−3171.
(67) Ishima, R.; Nagayama, K. *J. Magn. Reson., Ser. B* **1995**, *108*, 73−76.
(68) Trott, O.; Palmer, A. G. *J. Magn. Reson.* **2002**, *154*, 157−160.

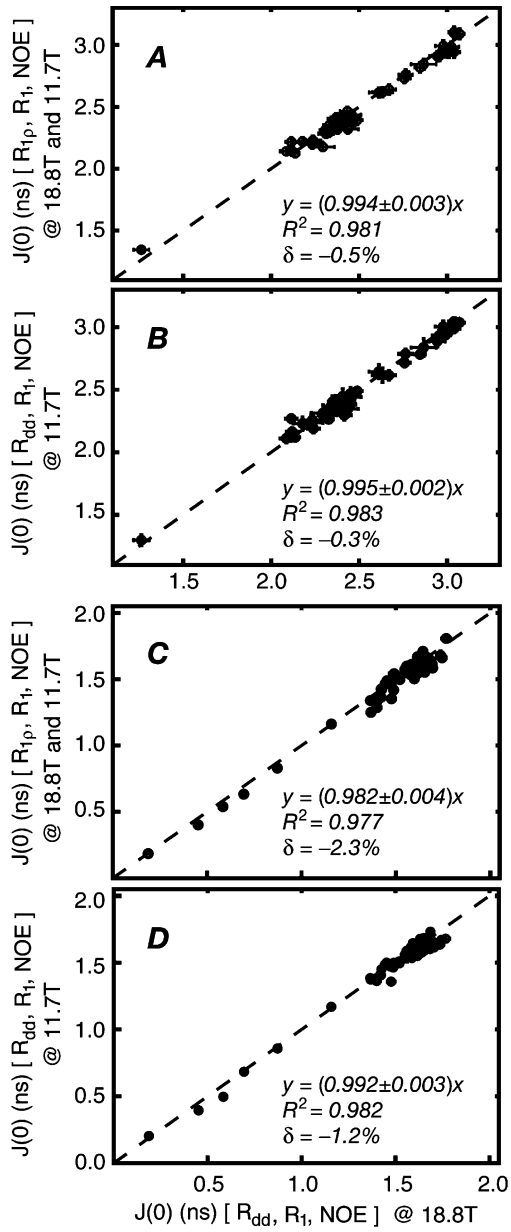

Figure 5. (A, C) $J(0)$ values obtained from measurements of $^1H-^{15}N$ R_{dd}, ^{15}N R_1, and $^1H-^{15}N$ NOE values at *one* static magnetic field strength agree with corresponding values isolated from ^{15}N R_1,^{15}N $R_{1\rho}$, and $^1H-^{15}N$ NOE measurements at *two* static magnetic fields for perdeutrated, ^{15}N labeled protein L, 278 K (*A*, $\tau_c \approx 8$ ns) and perdeutrated, ^{15}N labeled ubiquitin, 298 K (*C*, $\tau_c \approx 4.5$ ns). (B, D) $J(0)$ values obtained from measured $^1H-^{15}N$ R_{dd}, ^{15}N R_1, and $^1H-^{15}N$ NOE rates are independent of the static magnetic field strength for both protein L (B) and ubiquitin (D). The fitted slopes are obtained by a least-squares fit of the function $y = ax$ to the data, R is the coefficient of linear correlation, $R = \sigma_{xy}/(\sigma_{yy}\sigma_{xx})$, where $\sigma_{\nu\mu} = \sum(\nu_i - \langle\nu\rangle)(\mu_i - \langle\mu\rangle)/N$, N is the number of points, and δ is the systematic deviation from $y = x$, $\delta = \sum(y_i - x_i)/x_i$. The dashed lines correspond to $y = x$.

a significant advantage with an approach based on recording R_{dd} is that data from only a single field are required, while if the traditional methodology based on measurement of $R_{1\rho}$ rates is to be used relaxation data at a minimum of two fields must be generated and a model of how R_{ex} varies with B_0 must be evoked (see below) or the B_0 dependence of R_{ex} fit as an additional parameter.[69]

As a second validation we have compared $J(0)$ values obtained by independent mapping of $\{^{15}N$ R_1, $^1H-^{15}N$ R_{dd}, $^1H-^{15}N$ NOE$\}$ measured at a pair of static magnetic fields, 18.8 T and 11.7 T. Values of $J(0)$ are expected to be field independent, and indeed Figure 5B and D show that this is the case for both protein L and ubiquitin, respectively.

As a final note we wish to emphasize that we prefer to calculate R_{dd} rates from β (see above) rather than by fitting the decays of $2H'_zN_z$, $2H_zN'_z$, $2H'_zN'_z$, and $2H_zN_z$ separately and then taking the appropriate linear combinations of rates (eq 10) because effects due to cross-relaxation with external protons, modulations from scalar couplings, or imperfect spin-locking of magnetization tend to cancel to some extent by obtaining R_{dd} by fitting to a ratio of intensities. In addition, any interplay between A and R in fits of data to $y = A\exp(-RT_{relax})$ is minimized when R_{dd} is obtained from one rather than four fits.

Both the theoretical and experimental results presented above establish that to an excellent approximation the R_{dd} rate calculated from the measured value of $R_{\Sigma,\rho}$ and eq 11 depends only on the dipole−dipole $^1H-^{15}N$ interaction, with contributions from chemical exchange, CSA relaxation, and interactions with external spins canceling out, so long as reasonably high levels of deuteration are employed. This has particularly important advantages in applications to protein systems with pervasive chemical exchange, such as for a stabilized folding intermediate of the redesigned apocytochrome b_{562} protein,[29,34] considered below.

Dynamics of *PUF1:** The folding properties of redesigned apocytochrome b_{562} have been studied in some detail by a variety of biophysical approaches including native state hydrogen exchange experiments.[30] Using this method it has been shown that the folding pathway of this protein includes a pair of intermediates, *PUF2* where the N-terminal helix is not formed and *PUF1* where both N- and C-terminal helices are unstructured, $U \rightleftharpoons PUF1 \rightleftharpoons PUF2 \rightleftharpoons F$, and that the rate-limiting step is between the unfolded state, *U*, and *PUF1*[70]. Mutants have been designed to stabilize each of the two intermediates so that they can be studied directly.[29,33] In particular, mutations were generated in the N-terminal helix that have little effect on *PUF2*, *PUF1*, or *U* but that destabilize *F* (W7D, L10G, L14G, V16G, I17G), so that *PUF2* becomes the ground state. An additional three mutations were made (I98G, Y101G, Y105G) to convert *PUF1* to the ground state.[29] Here we examine the dynamics of the "stabilized" *PUF1* (i.e., where mutations are introduced to convert *PUF1* to the dominant state in solution, referred to in what follows as *PUF1**) that displays a wide range of motion over many time scales (see below), independent of protein concentration, and it is immediately clear even from a preliminary analysis of the dynamics data that there are pervasive contributions to relaxation from millisecond chemical exchange events. This can be seen in Figure 6 that shows the decay curves for $2H'_zN_z$ (△), $2H_zN'_z$ (▽), $2H'_zN'_z$ (□), and $2H_zN_z$ (○) elements measured for Asp 50 (A) and Val 69 (B) of *PUF1**, recorded at a static magnetic field of 14.1 T and a temperature of 288 K. The insets to the figure show the time dependence for $\beta = A_{SQ}(T_{relax})/A_{MQ,ZQ}(T_{relax})$ (see above), from which R_{dd} values are obtained. In the case of Asp 50, $R_{1\rho}(2H'_zN_z) \approx R_{1\rho}(2H_zN'_z) \approx R_{1\rho^2}(2H'_zN'_z) > R_1(2H_zN_z)$. Although the rate of the longitudinal order term is expected to be less than the others, the fact that

(69) Zhuravleva, A. V.; Korzhnev, D. M.; Kupce, E.; Arseniev, A. S.; Billeter, M.; Orekhov, V. Y. *J. Mol. Biol.* **2004**, *342*, 1599−1611.

(70) Zhou, Z.; Huang, Y. Z.; Bai, Y. W. *J. Mol. Biol.* **2005**, *352*, 757−764.

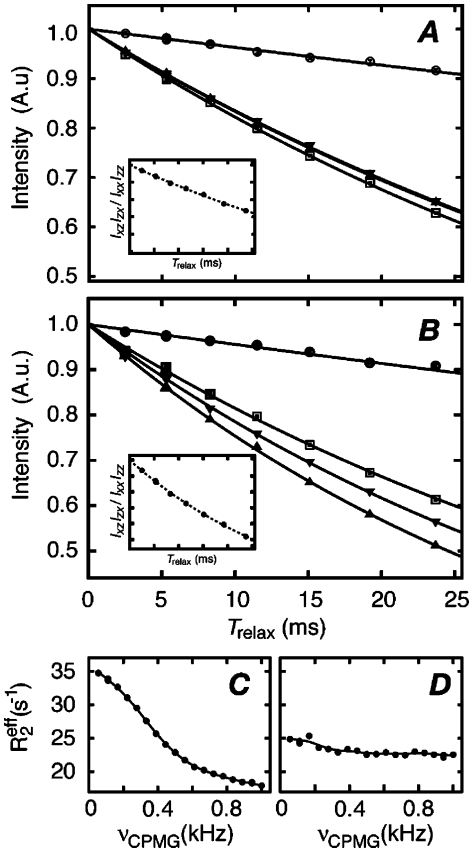

Figure 6. Decay curves of $2H_zN_z$ (○, $I_{zz}(T_{relax})$), $2H'_zN'_z$ (□, $I_{xx}(T_{relax})$), $2H_zN'_z$ (▽, $I_{zx}(T_{relax})$), and $2H'_zN_z$ (△, $I_{xz}(T_{relax})$) for Asp 50 (A) and Val 69 (B) of *PUF1**, 14.1 T, 288 K, obtained using the pulse schemes of Figure 1. The insets show the time dependence of the product $A_{SQ}(T_{relax})/A_{MQ,ZO}(T_{relax}) = I_{zx}(T_{relax}) \times I_{xz}(T_{relax})/[I_{xx}(T_{relax}) \times I_{zz}(T_{relax})]$ that decays with the rate constant $2R_{dd} \sin^2 \theta_H \sin^2 \theta_N$, eq 11.2. The solid lines are obtained from best-fits to an exponential decay function. Values of $R_1(2H_zN_z) = 3.79 \pm 0.08\ s^{-1}$ [$4.49 \pm 0.15\ s^{-1}$], $R_{1\rho^2}(2H'_zN'_z) = 19.62 \pm 0.07\ s^{-1}$ [$20.45 \pm 0.19\ s^{-1}$], $R_{1\rho}(2H'_zN_z) = 18.26 \pm 0.05\ s^{-1}$ [$28.25 \pm 0.12\ s^{-1}$], $R_{1\rho}(2H_zN'_z)$=$18.08 \pm 0.12\ s^{-1}$ [$24.15 \pm 0.18\ s^{-1}$] and $R_{dd} = 6.46 \pm 0.07\ s^{-1}$ [$13.77 \pm 0.10\ s^{-1}$] are obtained for Asp 50 [Val 69]. Relaxation dispersion profiles for residues Asp 50 (C) and Val 69 (D), along with fits to a two-site exchange process (solid lines).

all three coherences relax with similar rates can only be explained in terms of a chemical exchange process that contributes significantly to the measured decays. By contrast, the decay profiles for Val 69 are in keeping with expectations for a $^1H-^{15}N$ spin system in a perdeuterated protein when the contributions from chemical exchange processes are small, $R_1(2H_zN_z) < R_{1\rho^2}(2H'_zN'_z) < R_{1\rho}(2H_zN'_z) < R_{1\rho}(2H'_zN_z)$, eqs 1−4, 7−9. An indication of the relative importance of chemical exchange to the relaxation rates of coherences derived from residues Asp 50 and Val 69 is provided in Figure 6C and D, respectively, where ^{15}N relaxation dispersion profiles are illustrated. Large variations in relaxation rates, R_2^{eff}, as a function of the number of refocusing pulses applied during a constant-time relaxation interval[35] ($\nu_{CPMG} = 1/(2\delta)$, where δ is the delay between pulses) are a strong indication of exchange contributions on the millisecond time scale to the decay of (in this case ^{15}N) transverse magnetization. It is clear that such contributions are present for Asp 50 and only very slightly present for Val 69, as expected from the above discussion.

Values of R_{dd} have been obtained for 89 of the possible 101 backbone amide positions in *PUF1** and used along with values for ^{15}N R_1, $^1H-^{15}N$ NOE, and the NMR derived structure of the protein[29] to obtain diffusion parameters via the ModelFree program.[71] Figure 7A shows the lowest-energy NMR structure of *PUF1** (PDB: 1YZC(model 1))[29] along with the derived orientation of the diffusion tensor, based on data from the structured regions of the protein, as described in the legend. As expected $D_{||}$ is nearly collinear with the long axis of the protein. Values of S^2 and τ_e have been obtained using the diffusion tensor and measured {^{15}N R_1, $^1H-^{15}N$ R_{dd}, $^1H-^{15}N$

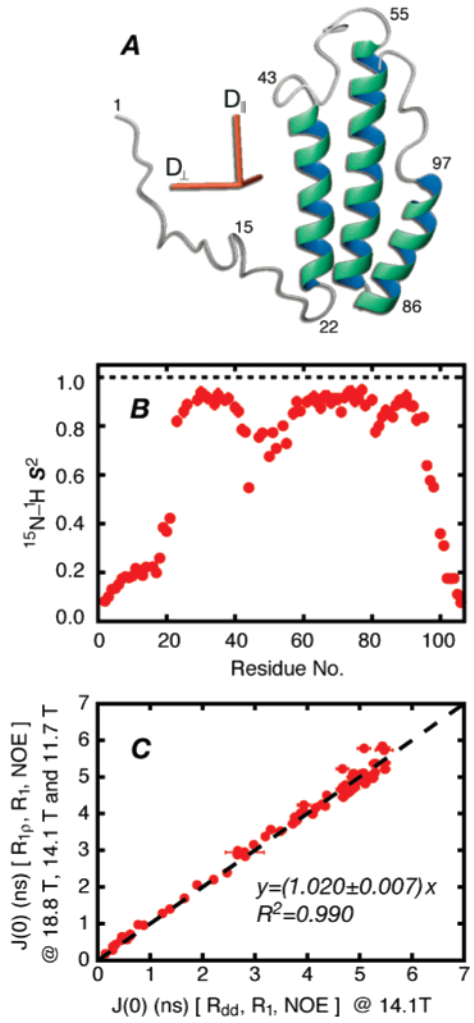

Figure 7. (A) The principal axis of the diffusion tensor of *PUF1** is collinear with the two major helices of the folding intermediate. The diffusion tensor has been determined as described in the text using {^{15}N R_1, $^1H-^{15}N$ R_{dd}, $^1H-^{15}N$ NOE}$_{14.1T}$ rates from residues 25−42, 58−80, and 84−95 (14.1 T, 288 K) that form helices in *PUF1**.[29] The obtained diffusion tensor parameters are as follows: $D_{iso} = (D_{||} + 2D_\perp)/3 = 1.53 \times 10^7\ s^{-1}$ ($\tau_{iso} = 10.8$ ns), $D_{||}/D_\perp = 2.02$, with the orientation of the unique axis of the tensor given by the polar angles $(\theta,\phi) = (85°,105°)$ in the PDB coordinate frame of the lowest-energy structure of the NMR ensemble (PDB: 1YZC(model 1)[29]). A diffusion tensor was also calculated from the {^{15}N R_1, ^{15}N $R_{1\rho}$, $^1H-^{15}N$ NOE}$_{11.7T,14.1T,18.8T}$ rates (see text) with $D_{iso} = (D_{||} + 2D_\perp)/3 = 1.56 \times 10^7\ s^{-1}$ ($\tau_{iso} = 10.7$ ns), $D_{||}/D_\perp = 1.97$ and $(\theta,\phi) = (83°,108°)$. (B) Order parameters, S^2(288 K) vs residue number, where the order parameters were derived from the {^{15}N R_1, $^1H-^{15}N$ R_{dd}, $^1H-^{15}N$ NOE}$_{14.1T}$ rates as described in the text. A simple two-parameter (S^2,τ_e) model-free spectral density function[20] was employed in the analysis. (C) $J(0)$ values obtained from measured {^{15}N R_1, $^1H-^{15}N$ R_{dd}, $^1H-^{15}N$ NOE}$_{14.1T}$ relaxation parameters agree with the corresponding spectral density values isolated from {^{15}N R_1,^{15}N $R_{1\rho}$, and $^1H-^{15}N$ NOE}$_{11.7T,14.1T,18.8T}$ parameters for perdeutrated, ^{15}N labeled *PUF1**, 288 K; the dashed line is $y = x$.

(71) Palmer, A. G. *ModelFree* **1998**, *4*, 16.

NOE}$_{14.1T}$ values, with S^2 plotted as a function of residue number in Figure 7B. A separate analysis has been carried out using conventional ^{15}N relaxation rates {^{15}N R_1, ^{15}N $R_{1\rho}$, ^{1}H−^{15}N NOE}$_{11.7T}$, {^{15}N R_1, ^{15}N $R_{1\rho}$, ^{1}H−^{15}N NOE}$_{14.1T}$, and {^{15}N R_1, ^{15}N $R_{1\rho}$, ^{1}H−^{15}N NOE}$_{18.8T}$ measured at three static magnetic field strengths of 11.7, 14.1, and 18.8 T, respectively. The nine rates were mapped onto seven spectral density values[65] and an exchange term, {$J(0)$, $J(\omega_{N,11.7T})$, $J(\omega_{N,14.1T})$, $J(\omega_{N,18.8T})$, $J(0.87\omega_{H,11.7T})$, $J(0.87\omega_{H,14.1T})$, $J(0.87\omega_{H,18.8T})$, R_{ex}}, assuming that R_{ex} is proportional to B_0^2. Exchange-free values of ^{15}N $R_{1\rho}$ were subsequently recalculated and used along with ^{15}N R_1 and ^{1}H−^{15}N NOE values to obtain the diffusion tensor following standard procedures.[72,73] Finally, the $J(0)$ values derived from the nine rates {^{15}N R_1, ^{15}N $R_{1\rho}$, ^{1}H−^{15}N NOE}$_{11.7T,14.1T,18.8T}$ were compared on a per-residue basis with the corresponding values obtained from reduced spectral density mapping of {^{15}N R_1, ^{1}H−^{15}N R_{dd}, ^{1}H−^{15}N NOE}$_{14.1T}$ (eq 13), Figure 7C. A strong correlation is obtained between $J(0)$ values derived from either $R_{1\rho}$ or R_{dd} rates, and consequently the diffusion tensors generated by the two methods are in excellent agreement. Thus, the assumption that $R_{ex} \propto B_0^2$ is reasonable for the analysis of relaxation data from this protein. It is worth noting that analysis of ^{15}N R_1, ^{15}N−^{1}H $R_{1\rho}$, ^{1}H−^{15}N NOE data derived from a single static magnetic field failed; the diffusion tensor determined did not agree well with that shown in Figure 7, and values of S^2 were larger than those plotted in Figure 7b, with $S^2 > 1$ in many cases.

Despite the fact that $R_{ex} \propto B_0^2$ for *PUF1** there are cases when this assumption is not strictly correct (see below), and here systematic errors can be introduced into the derived dynamics parameters using an analysis based on ^{15}N $R_{1\rho}$ values. For example, consider exchange between two states, A and B, with $p_A \gg p_B$. Trott and Palmer have derived an expression that relates R_{ex} to the exchange parameters,[68]

$$R_{ex} = \frac{p_A p_B \Delta\omega^2 k_{ex}}{\omega_{B,eff}^2 \omega_{A,eff}^2/\omega_{eff}^2 + k_{ex}^2} \approx \frac{p_A\, p_B \Delta\omega^2 k_{ex}}{\Omega_B^2 + \omega_1^2 + k_{ex}^2} \qquad (14)$$

where $\omega_{i,eff}^2 = \Omega_i^2 + \omega_1^2$, $\omega_{eff}^2 = (p_A\Omega_A + p_B\Omega_B)^2 + \omega_1^2$, $\Delta\omega = \Omega_A - \Omega_B$, with Ω_A and Ω_B the offsets of the ^{15}N resonance frequencies of the major and minor states from the carrier (rad/s), ω_1 is the field strength of the spin-lock field (rad/s), and k_{ex} is the rate of chemical exchange. Although the numerator of eq 14 increases with B_0^2, one of the three terms in the denominator (Ω_B^2) grows with B_0^2 as well; thus the field dependence of R_{ex} is expected to be somewhat less than quadratic unless $\omega_1^2 + k_{ex}^2 \gg \Omega_B^2$. Indeed, using two-site exchange parameters that characterize the folding/unfolding kinetics of the G48M Fyn SH3 domain (at 25−35 °C) that has been studied by our laboratory previously,[27] along with a ^{15}N spin-lock field of 1.9 kHz centered at 119 ppm, we calculate that $R_{ex,18.8T}/R_{ex,11.7T} = (18.79/11.74)^k$, with k varying between 1.8 and 2.0, depending on the residue. Clearly, in a general case, systematic errors will be introduced into the analysis of relaxation data if the assumption that $R_{ex} \propto B_0^2$ is made. As an illustration we have taken rates and chemical shift differences obtained from two-site fits of ^{15}N relaxation dispersion data recorded for the Fyn SH3 domain

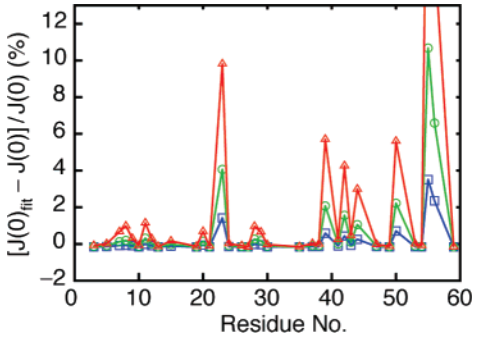

Figure 8. Systematic errors in the determination of $J(0)$ (or S^2) from the analysis of simulated relaxation data that is subsequently interpreted with the assumption that $R_{ex} \propto B_0^2$. The effects of chemical exchange were included using specific exchange parameters and chemical shifts that have been obtained from fits of ^{15}N relaxation dispersion data recorded on the G48M Fyn SH3 domain mutant[27] using eq 14; a two-site folding process is assumed. ^{15}N R_1, ^{15}N $R_{1\rho}$, and ^{1}H−^{15}N NOE values were computed at magnetic field strengths of 11.7 and 18.8 T. For all simulations, the spectral density function used to calculate the relaxation rates was described by a simple Lipari−Szabo model,[20] $J(\omega) = (^2/_5)[S^2\tau_R/(1 + \omega^2\tau_R^2) + (1 - S^2)\tau_e/(1 + \omega^2\tau_e^2)]$, where $S^2 = 0.8$ and $1/\tau_e = (1/100\text{ ps} + 1/\tau_R)$, and the spin-lock field strength in the $R_{1\rho}$ experiments was set to 1.9 kHz. Values of $J(0)_{fit}$ were determined from reduced spectral density mapping, {^{15}N R_1, ^{15}N $R_{1\rho}$ and ^{1}H−^{15}N NOE}$_{11.7T,18.8T}$ → {$J(0)$, $J(\omega_{N,11.7T})$, $J(\omega_{N,18.8T})$, $J(0.87\omega_{H,11.7T})$, $J(0.87\omega_{H,18.8T})$, R_{ex} ($R_{ex} \propto B_0^2$)}, and compared with the $J(0)$ used as input in the simulations. Data indicated by blue squares (□) are based on fits involving $R_{1\rho}$ values calculated from exchange parameters measured for the Fyn SH3 domain at 25 °C, i.e., $k_{ex} = 532\text{ s}^{-1}$, $p_B = 3.0\%$ along with $\tau_R = 5.0$ ns; green circles (○) correspond to parameters obtained at 30 °C, i.e., $k_{ex} = 851\text{ s}^{-1}$, $p_B = 4.5\%$ and $\tau_R = 4.35$ ns; while red triangles (△) are simulated with parameters obtained at 35 °C, i.e., $k_{ex} = 1362\text{ s}^{-1}$, $p_B = 6.2\%$, and $\tau_R = 3.9$ ns. Reliable ^{15}N relaxation dispersion profiles could be obtained experimentally at all temperatures for all the nuclei shown in the figure.

at a number of temperatures[27] and calculated $R_{1\rho}$ values at 18.8 and 11.7 T (assuming the set of dynamics parameters reported in the legend to Figure 8). Subsequently, simulated relaxation rates and NOE values were fitted to a model that assumes $R_{ex} \propto B_0^2$, and the extracted $J(0)$ values compared to those computed for the case where exchange contributions are set to zero. Figure 8 plots the systematic error in $J(0)$ values that is obtained for a series of exchange parameters that correspond to those obtained in the Fyn SH3 domain at temperatures ranging from 25 to 35 °C. For the Fyn system both k_{ex} and p_B increase with temperature, and since R_{ex} grows with p_B and k_{ex} (in the limit that $\omega_1 > k_{ex}$), systematic errors in $J(0)$ would also be expected to become larger at higher temperatures. This is indeed what is observed. Furthermore, systematic errors are expected to increase with decreasing effective correlation time, $\tau_{C,eff}$, since the relative contribution to transverse relaxation from chemical exchange increases (i.e., spin systems that are characterized by a shorter $\tau_{C,eff}$ will have smaller intrinsic exchange-free relaxation rates so that the relative contribution to the rates from exchange will increase). Thus, extra care must be taken when deriving $J(0)$ and S^2 for stabilized folding intermediates and disordered proteins, since these molecules can have large regions with short $\tau_{C,eff}$ values due to local flexibility. In addition, a second limitation of any model that assumes that R_{ex} is proportional to B_0^k is that it does not take into account potential differences in spin-lock field strengths between measurements

(72) Palmer, A. G.; Rance, M.; Wright, P. E. *J. Am. Chem. Soc.* **1991**, *113*, 4371−4380.
(73) Lee, L. K.; Rance, M.; Chazin, W. J.; Palmer, A. G. *J. Biomol. NMR* **1997**, *9*, 287−298.
(74) Massi, F.; Grey, M. J.; Palmer, A. G. *Protein Sci.* **2005**, *14*, 735−742.

performed at different static magnetic fields that only become insignificant in the limit that $\Omega_B^2 + k_{ex}^2 \gg \omega_1^2$ (eq 14). As a final point it is worth noting that exchange contributions for protein L and ubiquitin are such that $\omega_1^2 + k_{ex}^2 \gg \Omega_B^2$ [74] so that the assumption that R_{ex} is proportional to B_0^2 is reasonable for these proteins (Figure 5A,C).

Concluding Remarks

An approach is presented for obtaining an exchange-free measure of ^{15}N transverse relaxation, R_{dd}, that can be used in place of ^{15}N $R_{1\rho}$ rates in the study of internal protein dynamics. The method is based on the measurement of the relaxation of $^1H-^{15}N$ longitudinal order as well as a number of spin-locked $^1H-^{15}N$ coherences. Detailed simulations and experiments establish that R_{dd} values are independent of exchange, and for perdeuterated proteins systematic errors from dipolar interactions with proximal protons are calculated to be less than 1−2%, on average. Although we prefer to use proteins with very high levels of deuteration, the computations presented here establish that in applications involving proteins with deuteration levels in excess of 50% systematic errors under 4% can be anticipated. Systematic errors of this order are also observed in ^{15}N $R_{1\rho}$ measurements from contributions arising from external protons in fully protonated proteins. Measurements of R_{dd} values become particularly valuable in cases where exchange contributions are pervasive such as in studies of folded but unstable proteins, partially folded proteins, or folding intermediates. One such example of a stabilized folding intermediate of apocytochrome b_{562} has been presented here. Measurement of R_{dd} values that depend only on dipolar contributions to relaxation are likely to become increasingly important in studies performed at high magnetic fields where contributions from CSA to ^{15}N $R_{1\rho}$ rates become significant and hence site-by-site variations in CSA values begin to emerge as an issue.[75,76] The present set of experiments adds to a growing list of NMR methods that provides detailed information about protein dynamics that will ultimately lead to a far better understanding of the relation between motion and function in this important class of molecule.

Acknowledgment. This work is supported by a grant from the Canadian Institutes of Health Research (L.E.K). D.F.H. is the recipient of a postdoctoral fellowship from the Danish Agency for Science, Technology and Innovation (J. No. 272-05-0232). The authors thank Drs. Ranjith Muhandiram and Voula Kanelis for help with NMR experiments and sample preparation, respectively. L.E.K. holds a Canada Research Chair in Biochemistry.

Supporting Information Available: Description of the protocol used for computations of relaxation rates that include chemical exchange, along with plots showing that $J(0)$ extracted from the R_{dd} rate by reduced spectral density mapping is essentially independent of the CSA tensor. This material is available free of charge via the Internet at http://pubs.acs.org.

JA072717T

(75) Hall, J. B.; Fushman, D. *J. Am. Chem. Soc.* **2006**, *128*, 7855−7870.
(76) Burton, R. A.; Tjandra, N. *J. Biomol. NMR* **2006**, *35*, 249−259.